


Optimization of the Electric Arc Furnace Process

Yadollah Saboohi, Amirhossein Fathi, Igor Škrjanc , and Vito Logar 

Abstract—This paper presents an electric arc furnace (EAF) optimization framework intended to define optimal control profiles for the EAF, in order to increase its efficiency and thus reduce the energy consumption. The framework aims to minimize controllable losses and to maximize energy transfer to the bath and, consequently, minimize the operational costs. This is achieved through improved actuation of the EAF inputs, i.e., transformer power, oxygen lancing, and carbon addition. To achieve maximal energy transfer to the bath and to reduce the heat losses from the arcs, proper properties of the slag, such as foaminess and basicity, are a subject of considerable attention. The framework is designed as a model-based optimization, intended to be executed online in parallel to the actual EAF process. In order to achieve sufficiently low computational complexity and to allow process optimization by arbitrary time intervals, the framework uses path constraints instead of end-point constraints. A combination of several optimization algorithms is used to solve the optimization problem. The validation of the framework was performed by comparing the predicted and the measured operational variables. Simulation results show that optimized operation profiles lead to a significant decrease in operational costs and production times.

Index Terms—Dynamic optimization, electric arc furnace (EAF), online optimization, optimization problem modeling, profile optimization.

I. INTRODUCTION

ELECTRIC arc furnaces (EAFs) are used in the steel-making industry to produce a wide range of steel grades. As the production of steel in EAFs is considerably cheaper as in basic oxygen furnaces, in the last forty years, the amount of the steel produced in EAFs has grown from 100 to 430 million tons [1]. Since their beginning, the performance of the EAFs has been considerably improved. Introduction of several advanced technologies, such as off gas [2], [3] and slag [2], [4]

Manuscript received June 1, 2018; revised August 22, 2018, September 12, 2018, and September 26, 2018; accepted September 28, 2018. Date of publication December 3, 2018; date of current version May 31, 2019. This work was supported in part by the Slovenian Research Agency (ARRS) under Project J7-7197, and in part by the Sharif Energy Institute (SERI) under Project “Simulation and control of an EAF”. (Corresponding author: Vito Logar.)

Y. Saboohi and A. Fathi are with the Sharif Energy Research Institute, Sharif University of Technology, Tehran 11365-11155, Iran (e-mail: saboohi@sharif.edu; fathi@seri.sharif.edu).

I. Škrjanc and V. Logar are with the Laboratory of Autonomous Mobile Systems, Faculty of Electrical Engineering, University of Ljubljana, Ljubljana 1000, Slovenia (e-mail: igor.skrjanc@fe.uni-lj.si; vito.logar@fe.uni-lj.si).

Color versions of one or more of the figures in this paper are available online at <http://ieeexplore.ieee.org>.

Digital Object Identifier 10.1109/TIE.2018.2883247

heat recovery, post-combustion, gas burners [5], oxygen lancing [6], flexible alternating current transmission system instruments [7], high power transformers [8], and bottom stirring, have led to considerable decrease in energy consumption. A modern EAF uses 400–470 kWh/ton of electrical energy. Nonetheless, further improvements of the EAF operation are possible using different additives and heat recovery systems [9], [10] as well as improved control through optimized operational profiles.

A typical EAF is usually actuated according to the defined melting profiles, which are determined in advance and mostly rely to energy input and operator’s experience. To some extent, the profiles are designed to achieve the highest efficiency of the EAF; however, the predefined profiles do not consider fluctuating EAF conditions. Furthermore, proper actuation of the EAF is important to achieve appropriate slag characteristics, which reduce energy consumption and noise, protect the walls and water cooled panels, and contribute to the desired end-point steel composition. Due to limited insight into the EAF process, timely event onsets, such as charging, carbon injection, and oxygen lancing, usually deviate from ideal times and directly or indirectly lead to decreased EAF efficiency. For this reason, many studies investigating the EAF efficiency through optimized control have been performed. The studies mostly rely on mathematical models, which replicate the conditions inside the EAF. Optimization approaches are mainly focused on the reduction of the energy consumption and can be divided into four groups. The first group relates to the use of linear programming, such as the research from Cárdenas *et al.* [11] and Riesbeck *et al.* [12]. The second group is oriented toward model-predictive control, where studies of Bekker *et al.* [13], [14], Oosthuizen *et al.* [15], and Wei *et al.* [16] appear. The third group utilizes linear quadratic regulators to optimize the operation, such as the research from Bai [17] and Snell [18]. The last group uses various other approaches, such as the genetic algorithms (GAs) used by Czapla *et al.* [19], commercial software used by MacRosty and Swartz [20], [21] and Ghobara [22], and artificial neural networks used by Gajić *et al.* [23].

The literature review shows that only a few studies have been focused on the optimization of the energy carriers over tap-to-tap times (TTTs). The main reasons for that are probably two, i.e., optimization problem modeling, where the goals are poorly defined, and the implemented EAF models, which are often oversimplified to be included in the optimization problems. The used EAF models usually have the following drawbacks.

- 1) The lack of oxygen share estimation used to calculate the released energy from exothermic reactions, slag height, and masses of compounds and elements.
- 2) Numerical issues due to discrete charging of the EAFs.

- 3) The lack of heat transfer estimation due to variations in slag height, arc length, and bath height.
- 4) The lack of arc energy transfer estimation to other EAF zones as a function of arc length and arc current.

The implementation of dynamic optimization problems usually follows the same pattern, i.e., integration of an appropriate EAF model into the optimization problem, definition of constraints, and their implementation to the objective function. A set of differential algebraic equations (DAEs) can be used to define the optimization problem and can be solved using different methods and software. However, such framework is likely to be inefficient due to high computational loads caused by an infinite dimensional feasible region and discontinuities as a consequence of arc length, slag height, bath height, and input variations. The later may cause different heat transfer maps and can lead to nonconvex programming as a result of transferring DAE optimization to nonlinear optimization. The framework presented in this paper is intended to resolve these kinds of issues. In order to develop an efficient EAF optimization framework, a validated model [24] of a 105 ton EAF has been used together with the measured operational EAF data.

II. APPROACH

The aim of the presented optimization methodology is to propose an improved EAF operation that ensures the production of the steel with required characteristics in shorter time and with lower energy consumption in comparison to its past operations.

The proposed calculations are in many cases based on the so-called useful energy and useful power. The EAF produces one main product (steel) and many byproducts (slag and off-gas). The consumed energy is, therefore, distributed among the three and different losses; however, only the energy and power transferred to the steel bath can be considered as useful.

For the needs of solving the proposed optimization problem, the EAF operation is divided into four stages. The first stage starts at the beginning of the heat and lasts until minimal useful energy consumption is reached, which ensures proper bath temperature and mass at the beginning of stage four, assuming that the EAF is properly actuated during second and third stages. The second stage lasts until a semi-steady state is reached, which can be detected when the rate of change of slag height is approaching zero. The third stage is related to semi-steady stage operation and lasts until the refining (fourth) stage is achieved. The fourth stage is related to refining and lasts until proper bath temperature and composition are reached. The presented paper covers the first three stages of the optimization, which have different governing equations as the refining stage. Presenting and explaining the refining stage equations would excessively extend the paper; therefore, only short explanations of the refining stage optimization are given where necessary.

The objective function, used to maximize the useful energy profit per heat, consists of three measure indices, i.e., energy loss minimization, useful energy maximization, and operational cost minimization, forming a multiobjective optimization problem. The later can be transformed into a single-objective optimization by representing the first two objectives in monetary units. In this

TABLE I
EFFECT OF EAF INPUTS TO INCOMES IN THE OBJECTIVE FUNCTION

	income from			
	useful energy		material	
	direct effect	indirect effect		direct effect
through inputs		slag	Fe oxidation	Fe reduction
arc current				
arc length				
O ₂				
graphite				
C				

manner, the main goal of the objective function is to maximize the benefit over all inputs.

Control of the EAF inputs can have a direct or indirect effect on the incomes and costs related to the EAF operation as well as to the objective function. **Tables I** and **II** represent the effect of each input to the incomes and costs in the objective function.

As presented in **Tables I** and **II**, incomes and costs are related to energy and/or materials either being gained or lost. Thus, the incomes are related to the inputs that increase useful energy, such as arc currents and lengths, gas burners, and O₂, C, and graphite injection; and to the inputs that increase the mass of steel (higher yield), such as graphite and C injection for the decarburization process.

On the other hand, the costs are related to the inputs that result in the energy being lost, such as arc currents and lengths, and O₂, C, and graphite injection, whose part of the energy is subjected to losses to walls, roof, gas, and water-cooled panels through radiation and convection. The costs are also related to the inputs that decrease the mass of steel (lower yield), such as O₂ lancing in the iron oxidation process.

As known, each batch of produced steel needs to conform to the prescribed characteristics, needed to achieve a preferred grade, primarily end-point steel temperature and composition. Direct implementation of end-point constraints in optimization framework results in relatively long prediction horizons and, consequently, high computational complexity. For this reason, the presented solution proposes a replacement of end-point constraints with path constraints for the first three stages of the optimization. Path constraints ensure that conditions in an EAF at the beginning of stage four facilitate to achieve the desired end-point constraints when properly actuated. Implementation of path constraints on useful EAF power in the second and third stages is, thus, similar as implementation of an end-point constraint on temperature, however computationally significantly simpler.

The constraints, which need to be observed and satisfied, are composed of two groups, i.e., common constraints and exclusive constraints. The first group consists of technology-related limitations, such as input limitations (power and flows), arc resistances, and EAF volume. The second group consists of constraints for each stage of optimization, i.e., the first stage needs no specific constraints; second and third stages need a definition of useful power range; and the fourth stage needs a definition of end-point steel temperature and composition. Furthermore, limitations on slag quality are present at all four optimization

TABLE II
EFFECT OF EAF INPUTS TO COSTS IN THE OBJECTIVE FUNCTION

through input	cost for												material	purchase
	energy											direct effect		
	de-carburization	arc to wall	arc to roof	arc to water panels	arc to gas	slag to wall	slag to water panels	slag to roof	contained in slag					
arc current		rad	rad	rad	conv	conv	rad	conv	rad	conv	rad		Fe oxidation	
arc length														
O ₂														
graphite														
C														
slag added														

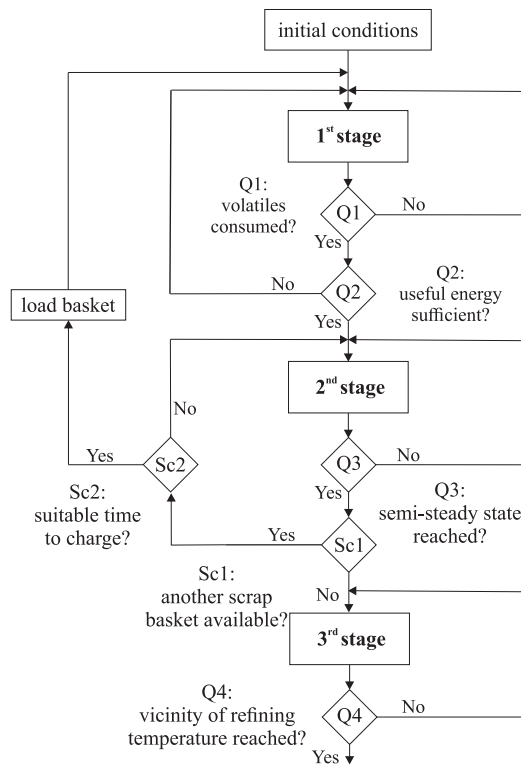


Fig. 1. Conceptual framework of optimal EAF control.

stages, which ensure proper quality and height of the slag. Minimal conditions to maintain foamy slag with appropriate basicity are continuously checked by estimating the oxide percentages in the slag while altering oxygen lancing and additive charging rates. At the same time, maximum carbon rates are calculated in order to maintain an acceptable bath composition at refining. Considering appropriate slag characteristics, other inputs can be optimized in order to maximize the defined performance measure. The concept of optimization framework is shown in Fig. 1.

Termination of each stage is determined according to different conditions, i.e., Q1, Q2, Q3, Q4, Sc1, and Sc2, where the role of each is as follows.

- 1) Q1 checks whether all volatile materials are consumed.
- 2) Q2 checks whether sufficient useful energy is provided in order to achieve sufficient tapping temperature (also

considering the energy loss during charging), assuming that all the following stages are properly actuated.

- 3) Q3 checks whether a semi-steady state of the operation is reached, i.e., derivative of slag height approaches zero.
- 4) Q4 checks whether the vicinity of the refining temperature is reached.
- 5) Sc1 checks whether another scrap basket is prepared for charging.
- 6) Sc2 estimates the suitable time to charge the prepared basket, i.e., sufficient amount of steel in the furnace has melted and useful furnace power is near the minimum acceptable value.

Fig. 2 schematically shows the structure of the optimization problem including the inputs to the EAF.

III. OPTIMIZATION PROBLEM MODELING

The following section describes the structure of the proposed optimization. In general, optimization is divided into three optimization problems, i.e., slag quality optimization in terms of its foaminess, energy transfer optimization, and slag quality optimization in terms of its basicity.

The notations used are similar as in our previous work [24], i.e., $Q_{(x-y)}$ represents the power transfer from zone x to zone y , where the studied EAF zones are arc (arcs), sSc (solid scrap), lSc (liquid scrap), sSl (solid slag), lSl (liquid slag), wall (brick), water (water cooled panels), roof (roof), elec (electrodes), and gas (gas). Superscripts of the variables represent the optimization step, and line superscripts ($\bar{\quad}$) of the variables show the average predicted variable during the step.

A. Slag Quality Optimization—Foaminess

The first part of the optimization problem relates to proper foaminess of the slag, which is needed to maintain the height of the slag as close as possible to the length of the arcs. Both excessive and insufficient slag amount lead to energy loss.

One way to predict the foaminess of the slag is to measure its content of iron oxide (FeO). In this manner, proper oxygen lancing can maintain the FeO between the upper and the lower limits. The cost of maintaining proper slag foaminess through oxygen lancing can be obtained as follows:

$$\text{Cost}_{\text{slag-foam}} = \text{Price}_{\text{O}_2} \text{O}_2^{i+1} t_s + M\gamma \quad (1)$$

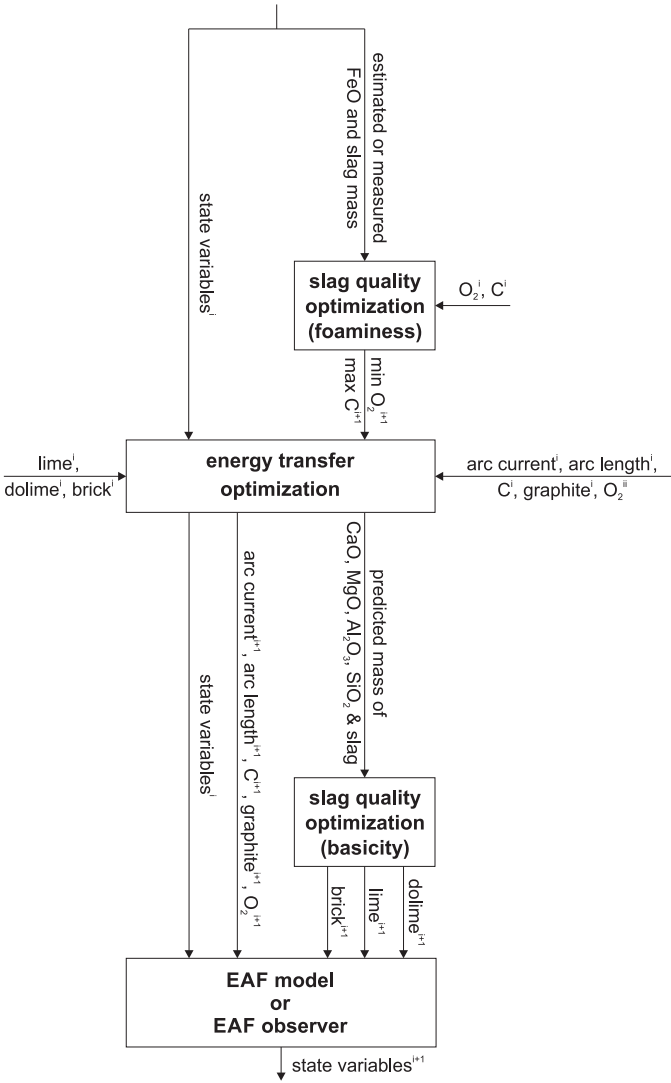


Fig. 2. Structure of the optimization problem.

and the rate of O_2 lancing can be obtained as follows:

$$\begin{aligned} \frac{\Xi_{O_2-FeO} O_2^{i+1} M_{O_2}}{2M_{FeO}} t_s + \frac{m_{FeO}}{m_{Slag}} + \gamma &> LB_{FeO} \\ \frac{\Xi_{O_2-FeO} O_2^{i+1} M_{O_2}}{2M_{FeO}} t_s + \frac{m_{FeO}}{m_{Slag}} - \gamma &\leq UB_{FeO} \\ O_2^i - \Delta O_2 &\leq O_2^{i+1} \leq O_2^i + \Delta O_2 \\ LB_{O_2} &\leq O_2^{i+1} \leq UB_{O_2} \\ \gamma &\geq 0 \end{aligned} \quad (2)$$

where $Cost_{slag-foam}$ represents the cost of consumed O_2 to maintain a desired FeO content in the slag, O_2^i represents O_2 lancing rate at step i , $Price_{O_2}$ represents the price of O_2 , and $M\gamma$ represents a penalty product, where M represents a large number, and γ represents a value that needs to be added to the calculation in order to satisfy the LB_{FeO} or UB_{FeO} constraint (the amount of FeO in slag) for short times. In this manner, nonfeasible

solutions, in case of shortage or excess of O_2 lancing, are avoided. Furthermore, Ξ_{O_2-FeO} represents a fraction of O_2 reacting with Fe to form FeO , M_{O_2} and M_{FeO} represent molar masses of O_2 and FeO , m_{FeO} and m_{Slag} represent the masses of FeO and slag, LB_{O_2} and UB_{O_2} represent lower and upper limits of O_2 lancing rate, ΔO_2 represents a permissible rate of change of O_2 lancing in each step, and t_s represents the sampling time.

Injection of carbon represents an important addition to the EAF process, which affects several processes during melting, slag foaming through CO among others. However, excessive C injection can lead to surpassed C content in the bath at tapping. Therefore, the maximum carbon rate should be limited not to exceed its maximum acceptable percentage at the end of the TTT. The condition in order to obtain the maximum carbon injection rate in each optimization step is shown as follows:

$$\text{Max} \sum_{j=1}^{\left(\frac{TTT}{t_s}\right)-i} C_{inj}^{i+i_p} \quad (3)$$

where $C_{inj}^{i+i_p}$ represents the prediction of the C injection rate in the future (i_p steps further from the current step i). The conditions that need to be satisfied are given as follows:

$$\begin{aligned} C_{charged} + C_0 - \int_0^{TTT} (\dot{m}_{C-L} + \dot{m}_{C-D}) dt &\leq UB_{CinSteel} \\ C_{inj}^{i+i_p-1} - \Delta C_{inj} &\leq C_{inj}^{i+i_p} \leq C_{inj}^{i+i_p-1} + \Delta C_{inj} \\ LB_{Cinj} &\leq C_{inj}^{i+i_p} \leq UB_{Cinj} \\ 1 \leq i_p &\leq \left(\frac{TTT}{t_s}\right) - i \end{aligned} \quad (4)$$

where $C_{charged}$ represents the charged C , C_0 represents the initial C contained in scrap, \dot{m}_{C-L} and \dot{m}_{C-D} represent the consumed C that was injected or already dissolved, respectively [24], $UB_{CinSteel}$ represents the maximum acceptable amount of C at tapping, ΔC_{inj} represents a permissible rate of change of C injection in each step, and LB_{Cinj} and UB_{Cinj} represent the lower and the upper limits of C injection rate.

B. Energy Transfer Optimization

The second part of the optimization problem relates to the definition of optimal energy input, with respect to both limitations for this optimization level and also on carbon and oxygen additions defined in the previous section.

The objective function is a combination of income sums and cost sums represented by each of the inputs described as follows:

$$\text{max} \sum_{in} \left(\sum_n \text{Income}_{in} - \sum_m \text{Cost}_{in} \right) \quad (5)$$

where in represents the input, n represents all incomes from input in , and m represents all costs from input in . The contribution of each input to the objective function is obtained according to Tables I and II and the following equations.

The price of useful energy (P_{UP}) used in several equations is determined according to the scrap price (P_{Sc}), molten steel

price at the beginning of the refining stage (P_{steel}) and the required useful energy (Υ) described as follows:

$$P_{\text{UP}} = \frac{P_{\text{Steel}} - P_{\text{sSc}}}{\Upsilon} \quad (6)$$

where the required useful energy Υ is calculated as a difference between the internal energy of the scrap at charging and the internal energy of the molten steel at the beginning of the refining stage.

Proper quality and height of the slag represent a crucial part in optimal EAF control. Fluctuations in its height lead to different dimensions of the interacting surfaces, i.e., contact areas between the slag and other zones, causing different energy transfers between them. Different heights of the slag also affect the view factors and the radiative heat transfers. Therefore, each change in the height of the slag leads to variations in incomes and costs of the objective function. Among others, the task of the optimization procedure is to find the optimal height of the slag, by controlling carbon and oxygen addition, in order to maximize the incomes and to minimize the costs.

In some equations, slag, despite its beneficiary effects to the EAF operation, appears as the cost when liquid slag is in contact with the side walls. In such case, the slag's internal energy, which could be transferred to the steel, is actually being lost to walls. This would not have happened if the slag was not in contact with the walls, regardless of its positive effects. The beneficial effect of the slag is taken into the account in income equations, where a proper height of the slag increases the incomes from the particular input and also reduces its costs, due to, e.g., less radiation.

The following five sections describe the contribution of each EAF input to the incomes and the costs in the objective function.

1) Contribution of Arc Length and Current: Shares of arc energy received by the scrap, slag, gas, wall, and roof can be estimated by two independent variables, i.e., arc length and arc current [24]. The income related to the arcs can be obtained as follows:

$$\text{Income}_{\text{arc}} = P_{\text{UP}} \left[Q_{\text{arc-IsC}} + \frac{1}{2} \eta_{\text{ISl-IsC}} Q_{\text{arc-ISl}} \right] t_s \quad (7)$$

where $Q_{\text{arc-IsC}}$ represents the arc power directly transferred to molten steel by conduction, $\eta_{\text{ISl-IsC}} Q_{\text{arc-ISl}}$ represents the arc power indirectly transferred to molten steel through the slag. One half of the indirect income is assumed to attribute to arc energy, while the other half of the arc energy is assumed to be consumed for the formation of the slag.

The costs related to the arcs can be obtained as follows:

$$\begin{aligned} \text{Cost}_{\text{arc}} = P_{\text{UP}} \eta_{\text{ISl-IsC}} [& Q_{\text{arc-wall}} + Q_{\text{arc-water}} \\ & + Q_{\text{arc-roof}} + Q_{\text{arc-gas}}] t_s + P_{\text{el}} Q_{\text{arc}} t_s \end{aligned} \quad (8)$$

where $\eta_{\text{ISl-IsC}}$ represents the percentage, which determines the amount of energy transferred from liquid slag to molten steel, $Q_{\text{arc-wall}}$, $Q_{\text{arc-water}}$, $Q_{\text{arc-roof}}$, and $Q_{\text{arc-gas}}$ represent the powers transferred from the arcs to walls, water-cooled panels, roof, and gas, P_{el} represents the price of electrical energy, and Q_{arc} represents the total power of the arcs.

2) Contribution of Carbonaceous Materials: Carbonaceous materials are usually used to reduce the FeO to Fe and increase the overall Fe yield. The incomes of carbonaceous materials are related to slag formation, which covers the arcs, to the released iron from decarburization reactions (higher yield) and also to the released energy of carbon oxidation and can be obtained as follows:

$$\begin{aligned} \text{Income}_C = & \left[\frac{1}{2} \eta_{\text{ISl-IsC}} P_{\text{UP}} Q_{\text{arc-ISl}} \frac{h_{\text{SlagC-arc}}^{i+1}}{h_{\text{arc}}^{i+1}} + P_{\text{steel}} \frac{M_{\text{Fe}}}{M_{\text{C}}} \right. \\ & + (P_{\text{UP}} \varphi_{C-\text{IsC}} + \eta_{\text{ISl-IsC}} P_{\text{UP}} (1 - \varphi_{C-\text{IsC}})) \\ & \left. \times C_{\text{inj}} K_{C-\text{O}_2}^{i+1} Q_{C-\text{O}_2}^{i+1} \right] t_s \end{aligned} \quad (9)$$

where h_{arc}^{i+1} represents the length of the arcs at the $i + 1$ step, $h_{\text{SlagC-arc}}^{i+1}$ represents the height of the slag at the $i + 1$ step, which is a consequence of C addition, $\varphi_{C-\text{IsC}}$ is a fraction of chemical power transferred to molten steel, $K_{C-\text{O}_2}^{i+1}$ represents a fraction of C, which reacts with O_2 , and $Q_{C-\text{O}_2}^{i+1}$ represents the released combustion power of C per kg.

The costs related to carbonaceous materials addition are a consequence of their purchase expenses, energy consumption due to endothermic reactions, and energy transfer from slag to walls, electrodes, and water-cooled panels and can be obtained as follows:

$$\begin{aligned} \text{Cost}_C = & \left[P_C (-\dot{m}_{c-\text{dec}}^{i+1}) + (\eta_{\text{ISl-IsC}} P_{\text{UP}} (1 - \varphi_{C-\text{IsC}}) \right. \\ & + P_{\text{UP}} \varphi_{C-\text{IsC}}) (-\dot{m}_{c-\text{dec}}^{i+1}) Q_{(C-\text{dec})} \\ & + \eta_{\text{ISl-IsC}} P_{\text{UP}} Q_{\text{ISl-wall}} \frac{h_{\text{SlagC}_2}^{i+1}}{h_{\text{Slag}}^{i+1}} \\ & + \eta_{\text{ISl-IsC}} P_{\text{UP}} Q_{(\text{ISl-elec})} \frac{h_{\text{SlagC}_3}^{i+1}}{h_{\text{Slag}}^{i+1}} \\ & \left. + \eta_{\text{ISl-IsC}} P_{\text{UP}} Q_{\text{ISl-water}} \frac{h_{\text{SlagC}_4}^{i+1}}{h_{\text{Slag}}^{i+1}} \right] t_s \end{aligned} \quad (10)$$

where P_C represents the price of the material, $\dot{m}_{c-\text{dec}}^{i+1}$ represents the change of mass of C consumed in the decarburization process as described by (11), $Q_{c-\text{dec}}$ represents the power needed for the decarburization process per kg of C, h_{Slag}^{i+1} represents the height of the slag at the $i + 1$ step, $h_{\text{SlagC}_2}^{i+1}$ represents the height of the slag formed by the decarburization process covering the walls, $h_{\text{SlagC}_3}^{i+1}$ represents the height of the slag formed by the decarburization process covering the water cooled panels, and $h_{\text{SlagC}_4}^{i+1}$ represents the height of the slag formed by the decarburization process covering the electrodes.

3) Contribution of Graphite: The role of graphite in the objective function is similar to carbonaceous materials, with one major difference, i.e., it is assumed that graphite reacts much quicker and is, therefore, not oxidized. There are two factors when injecting graphite that affects the height of the slag, i.e., decarburization reaction and N_2 injection as the carrier gas,

where the decarburization rate can be assumed to be proportional to the graphite injection rate. The income of graphite addition is related to slag formation and increased steel yield and can be described as follows:

$$\text{Income}_{Gr} = \left[\frac{1}{2} \eta_{\text{SI-ISC}} P_{\text{UP}} Q_{\text{arc-ISI}} \frac{h_{\text{SlagGr-arc}}^{i+1}}{h_{\text{arc}}^{i+1}} + P_{\text{Steel}} \frac{M_{\text{Fe}}}{M_{\text{C}}} (\dot{m}_{\text{Gr}}^{i+1}) \frac{T_{\text{ISC}}^{i+1}}{T_{\text{des-ISC}}} \right] t_s \quad (11)$$

where $h_{\text{SlagGr-arc}}^{i+1}$ represents the height of the slag that covers the arcs and is a consequence of graphite injection, $\dot{m}_{\text{Gr}}^{i+1}$ represents graphite injection rate at the $i + 1$ step, and $T_{\text{des-ISC}}$ represents the desired tapping temperature.

The costs related to graphite addition are similar to other carbonaceous materials and can be described as follows:

$$\begin{aligned} \text{Cost}_{\text{Gr}} = & \left[P_{\text{Gr}} \dot{m}_{\text{Gr}}^{i+1} + (\eta_{\text{SI-ISC}} P_{\text{UP}} (1 - \varphi_{\text{C-ISC}}) \right. \\ & + P_{\text{UP}} \varphi_{\text{C-ISC}}) (-\dot{m}_{\text{Gr}}^{i+1}) Q_{\text{c-dec}} \\ & + \eta_{\text{SI-ISC}} P_{\text{UP}} Q_{\text{ISI-wall}} \frac{h_{\text{SlagGr}_2}^{i+1}}{h_{\text{Slag}}^{i+1}} \\ & + \eta_{\text{SI-ISC}} P_{\text{UP}} Q_{\text{ISI-elec}} \frac{h_{\text{SlagGr}_3}^{i+1}}{h_{\text{Slag}}^{i+1}} \\ & \left. + \eta_{\text{SI-ISC}} P_{\text{UP}} Q_{\text{ISI-water}} \frac{h_{\text{SlagGr}_4}^{i+1}}{h_{\text{Slag}}^{i+1}} \right] t_s \quad (12) \end{aligned}$$

where P_{Gr} represents the price of graphite, $h_{\text{SlagGr}_2}^{i+1}$ represents the height of the slag formed by the decarburization process (from graphite) covering the walls, $h_{\text{SlagGr}_3}^{i+1}$ represents the height of the slag formed by the decarburization process (from graphite) covering the water cooled panels, and $h_{\text{SlagGr}_4}^{i+1}$ represents the height of the slag formed by the decarburization process (from graphite) covering the electrodes.

4) Contribution of O₂ Lancing: The income of oxygen lancing is related to slag formation and released chemical energy from exothermic reactions, which is transferred to bath directly or indirectly through slag and can be described as follows:

$$\begin{aligned} \text{Income}_{\text{O}_2} = & \left[\frac{1}{2} \eta_{\text{SI-ISC}} P_{\text{UP}} Q_{\text{arc-ISI}} \frac{h_{\text{SlagO}_2\text{-arc}}^{i+1}}{h_{\text{arc}}^{i+1}} \right. \\ & + (P_{\text{UP}} \varphi_{\text{C-ISC}} + \eta_{\text{SI-ISC}} P_{\text{UP}} (1 - \varphi_{\text{C-ISC}})) \\ & \left. \times \left(\sum_{\text{el,el} \neq \text{C}} -\dot{m}_{\text{el-O}_2}^{i+1} Q_{\text{el-O}_2}^{i+1} \right) \right] t_s \quad (13) \end{aligned}$$

where $h_{\text{SlagO}_2\text{-arc}}^{i+1}$ represents the height of the slag that covers the arcs and is a consequence of oxygen lancing, $\dot{m}_{\text{el-O}_2}^{i+1}$ represents the change of O₂ mass consumed in oxidation of element el, and $Q_{\text{el-O}_2}$ represents the power per kg of O₂ released when element el is oxidized.

The costs related to oxygen lancing are a consequence of its purchase expenses, oxidation of different dissolved elements, oxidation of iron (lower yield), and energy transfer from molten steel to walls through the slag layer and can be described as follows:

$$\begin{aligned} \text{Cost}_{\text{O}_2} = & \left[P_{\text{O}_2} \text{O}_2 + \sum_{\text{el,el} \neq \text{C \& Fe}} \dot{m}_{\text{el-O}_2}^{i+1} P_{\text{el}} \right. \\ & + 2 P_{\text{Steel}} \frac{M_{\text{Fe}}}{M_{\text{O}_2}} K_{\text{O}_2\text{-FeO}} \text{O}_2 \frac{T_{\text{ISC}}^{i+1}}{T_{\text{des-ISC}}} \\ & + \eta_{\text{SI-ISC}} P_{\text{UP}} Q_{\text{ISI-wall}} \frac{h_{\text{SlagO}_2}^{i+1}}{h_{\text{Slag}}^{i+1}} \\ & + \eta_{\text{SI-ISC}} P_{\text{UP}} Q_{\text{ISI-elec}} \frac{h_{\text{SlagO}_3}^{i+1}}{h_{\text{Slag}}^{i+1}} \\ & \left. + \eta_{\text{SI-ISC}} P_{\text{UP}} Q_{\text{ISI-water}} \frac{h_{\text{SlagO}_4}^{i+1}}{h_{\text{Slag}}^{i+1}} \right] t_s \quad (14) \end{aligned}$$

where P_{el} represents the price of the element, $K_{\text{O}_2\text{-FeO}}$ represents a fraction of O₂, which reacts with Fe to form FeO, $h_{\text{SlagO}_2}^{i+1}$ represents the height of the slag formed by oxygen injection covering the walls, $h_{\text{SlagO}_3}^{i+1}$ represents the height of the slag formed by oxygen injection covering the water cooled panels, and $h_{\text{SlagO}_4}^{i+1}$ represents the height of the slag formed by oxygen injection covering the electrodes.

5) Contribution of Slag Forming Additives: In order to achieve the slag with desired characteristics, proper charging of the slag forming agents is necessary. Consequently, their charging represents two different costs in the objective function, i.e., purchase expenses $\text{Cost}_{\text{slag-P}}$ and energy consumption expenses $\text{Cost}_{\text{slag-E}}$, which are summed and divided by the remaining time of a certain heat described as follows:

$$\text{Cost}_{\text{slag}} = \frac{\text{Cost}_{\text{slag-P}} + \text{Cost}_{\text{slag-E}}}{t_{\text{remaining}}} \quad (15)$$

The purpose of dividing the slag costs by the remaining time is to limit the charging of the slag additives in the last moments of the heat. The purchase costs can be obtained as follows:

$$\begin{aligned} \text{Cost}_{\text{slag-P}} = & \left(h_{\text{Slag}}^{i+1} \rho_{\text{slag}} A_{\text{EAF}} - \sum_{\text{comp}} (\dot{m}_{\text{comp}}^i - \dot{m}_{\text{comp}}^{i+1}) t_s \right) \\ & \times \left(\sum_j \alpha_j P_j \right) \quad (16) \end{aligned}$$

where h_{Slag}^{i+1} represents the height of the slag at the $i + 1$ sample, ρ_{slag} represents the density of the foamy slag, A_{EAF} represents the EAF surface area, \dot{m}_{comp}^i represents the mass of the compound in the slag, $\dot{m}_{\text{comp}}^{i+1}$ represents the estimated change of compound mass to be added, α_j represents the share of additive j that needs to be charged, and P_j represents the price of the additive j . Additive j can be lime, dolime, or brick, and comp can be CaO, MgO, SiO₂, or Al₂O₃. Slag height, which is

a consequence of carbon, carbonaceous materials, and oxygen additions, can be obtained as follows:

$$h_{\text{slag}}^{i+1} = h_{\text{slagC}}^{i+1} + h_{\text{slagGr}}^{i+1} + h_{\text{slagO}_2}^{i+1}. \quad (17)$$

The costs of energy, which is needed to melt the charged additives, can be obtained as follows:

$$\begin{aligned} \text{Cost}_{\text{slag-E}} = \eta_{\text{Sl-Sc}} P_{\text{UP}} \left(h_{\text{slag}}^{i+1} \rho_{\text{slag}} A_{\text{EAF}} - \sum_{\text{comp}} m_{\text{comp}} \right) \\ \cdot \left[\sum_j \alpha_j \left(\int_{T_{\text{air}}}^{T_{\text{molten}}} C_{P-\text{solid}_j}(T) dT + \lambda_j \right. \right. \\ \left. \left. + \int_{T_{\text{molten}}}^{T_{\text{IS1}}} C_{P-\text{liquid}_j}(T) dT \right) \right] \quad (18) \end{aligned}$$

where $C_{P-\text{solid}_j}(T)$ represents the specific heat capacity of solid additive j at temperature T , λ_j represents the latent heat of fusion of additive j , and $C_{P-\text{liquid}_j}(T)$ represents the specific heat capacity for liquid additive j at temperature T .

C. Slag Quality Optimization—Basicity

The third part of the optimization problem relates to proper basicity of the slag, which can be achieved by adding different slag-forming agents, such as dolomite, lime, and brick. The amount of each additive to be added to achieve proper slag basicity and their influence on the costs can be determined by (19) and (20):

$$\text{Cost}_{\text{slag-bas}} = \sum_j \dot{m}_{j,2}^{i+1} P_j t_s + \sum_k M \gamma_k + \sum_k M \vartheta_k \quad (19)$$

where $\dot{m}_{j,2}^{i+1}$ represents the mass of additive j to achieve proper basicity at step $i+1$, P_j represents additive price, and $\dot{m}_{j,1}^{i+1}$ represents the mass of additive added in equations in

Section III-B5. Similar to (1), penalty products $M\gamma_k$ and $M\vartheta_k$ are defined in order to avoid infeasible solutions, where M represents a large number, and γ_k and ϑ_k represent a value that needs to be added to the calculation in order to satisfy the $\text{LB}_{\text{basicity}}$ and $\text{UB}_{\text{basicity}}$ constraints (lower and upper basicity value) in (20) as shown bottom of this page, where $\text{LB}_{\text{bas},k}$ and $\text{UB}_{\text{bas},k}$ represent the lower and the upper limit of slag quality criteria k , $\tilde{m}_{\text{comp}}^{i+1}$ represents the average mass of compound comp (CaO, MgO, SiO₂, or Al₂O₃) at step $i+1$, $\alpha_{j,\text{comp}}$ represents a share of compound comp in additive j , u_j^i and Δu_j represent the amount of additive j in step i and a maximum possible change for additive j , m_j^i represents a mass of additive j in step i , and LB_j and UB_j represent the lower and upper possible limit of additive j in slag. Observing (20), the first four constraints are based on different basicity measures, depending on the composition of the slag. For each heat optimization, one of the three constraints is used, and its selection depends on the expected slag composition. The fourth and the fifth constraints are used to determine the minimum MgO amount in the slag according to the current FeO content, in order to prevent increased corrosion rate of the walls due to higher slag temperature (fourth) and/or high FeO content (fifth).

D. Limitations

The limitations considered in the optimization framework are classified into two groups, i.e., common limitations, which are valid for all optimization stages and exclusive limitations, which are valid only for separate stages.

Common limitations are related to the installed technology constraints and are described as follows, which provide proper calculation of each input at each step:

$$\text{LB}_{\text{min}} \leq \text{LB}^{i+1} \quad (21)$$

$$u^i - \Delta u \leq \text{LB}^{i+1} \quad (22)$$

$$\begin{aligned} \text{LB}_{\text{bas},1} &\leq \gamma_1 + \frac{\tilde{m}_{\text{CaO}}^{i+1} + \sum_j \alpha_{j,\text{CaO}} \dot{m}_{j,2}^{i+1} t_s}{\tilde{m}_{\text{SiO}_2}^{i+1} + \sum_j \alpha_{j,\text{SiO}_2} \dot{m}_{j,2}^{i+1} t_s} - \vartheta_1 \leq \text{UB}_{\text{bas},1} \\ \text{LB}_{\text{bas},2} &\leq \gamma_2 + \frac{\tilde{m}_{\text{CaO}}^{i+1} + \sum_j \alpha_{j,\text{CaO}} \dot{m}_{j,2}^{i+1} t_s}{\tilde{m}_{\text{SiO}_2}^{i+1} + \sum_j \alpha_{j,\text{SiO}_2} \dot{m}_{j,2}^{i+1} t_s + \tilde{m}_{\text{Al}_2\text{O}_3}^{i+1} + \sum_j \alpha_{j,\text{Al}_2\text{O}_3} \dot{m}_{j,2}^{i+1} t_s} - \vartheta_2 \leq \text{UB}_{\text{bas},2} \\ \text{LB}_{\text{bas},3} &\leq \gamma_3 + \frac{\tilde{m}_{\text{CaO}}^{i+1} + \sum_j \alpha_{j,\text{CaO}} \dot{m}_{j,2}^{i+1} t_s + \tilde{m}_{\text{MgO}}^{i+1} + \sum_j \alpha_{j,\text{MgO}} \dot{m}_{j,2}^{i+1} t_s}{\tilde{m}_{\text{SiO}_2}^{i+1} + \sum_j \alpha_{j,\text{SiO}_2} \dot{m}_{j,2}^{i+1} t_s + \tilde{m}_{\text{Al}_2\text{O}_3}^{i+1} + \sum_j \alpha_{j,\text{Al}_2\text{O}_3} \dot{m}_{j,2}^{i+1} t_s} - \vartheta_3 \leq \text{UB}_{\text{bas},3} \\ 0.02567 T_{\text{IS1}}^{i+1} - 35.71 - \vartheta_5 &\leq \tilde{m}_{\text{MgO}}^{i+1} + \sum_j \alpha_{j,\text{MgO}} \dot{m}_{j,2}^{i+1} t_s \\ 0.0112 \text{FeO}\% - 0.3673 \text{FeO}\% + 9.221 - \vartheta_6 &\leq \tilde{m}_{\text{MgO}}^{i+1} + \sum_j \alpha_{j,\text{MgO}} \dot{m}_{j,2}^{i+1} t_s \\ u_j^i - \Delta u_j &\leq (\dot{m}_{j,1}^{i+1} + \dot{m}_{j,2}^{i+1}) t_s + m_j^i \leq u_j^i + \Delta u \\ \text{LB}_j &\leq (\dot{m}_{j,1}^{i+1} + \dot{m}_{j,2}^{i+1}) t_s + m_j^i \leq \text{UB}_j \\ \gamma_k, \vartheta_k &\geq 0 \end{aligned} \quad (20)$$

$$UB^{i+1} \leq UB_{\max} \quad (23)$$

$$UB^{i+1} \leq u^i + \Delta u \quad (24)$$

$$LB^{i+1} \leq u^{i+1} \leq UB^{i+1} \quad (25)$$

where LB_{\min} and UB_{\max} represent the minimum and the maximum possible vector of inputs, LB^{i+1} and UB^{i+1} represent the minimum and the maximum vector of inputs at step $i + 1$, u^i represents the vector of inputs at step i , and Δu represents the maximum change vector of inputs.

Exclusive limitations are related to the desired result of the optimization and are used to replace the end-point constraints, such as molten mass and temperature, in order to reduce the computational load. For this reason, path constraints are introduced in second and third stages of the optimization process and can be described as follows:

$$LB_{UP}^{i+1} \leq Q_{lSc}^{i+1} + Q_{sSc}^{i+1} \leq UB_{UP}^{i+1} \quad (26)$$

where LB_{UP} and UB_{UP} represent the lower and the upper useful power limit calculated at each step, and Q_{lSc}^{i+1} and Q_{sSc}^{i+1} represent the powers transferred to liquid and solid scrap zones.

E. Optimization Solver and Used Prices

The proposed optimization problem is defined using a combination of the objective function and the constraints. During the heat, the equations defining the optimization problem are changing due to varying conditions in the EAF; therefore, leading to different optimization spaces. If only one optimization method is applied, it is possible that an infeasible solution is found, i.e., leading to infeasible EAF operation. Therefore, to overcome this drawback, multiple solvers are used simultaneously, and feasibility of each solution is checked in each optimization step. The results presented in this paper are obtained using a combination of the following MATLAB solvers: GAs, SQP, Active set, Trust region reflective, and Interior point, the last four being the algorithms from the constrained nonlinear optimization algorithms.

Prices of raw materials, energy, and additives as used in the objective function are the following: electrical energy—0.15 \$/kWh, O_2 —0.1 \$/Nm³, C—0.28 \$/kg, graphite—2 \$/kg, scrap—0.2 \$/kg, and crude liquid steel—0.6 \$/kg.

IV. RESULTS

The following section presents simulation results of the optimization algorithm performing the first three stages of the optimization. In order to demonstrate the improvement of EAF control when using the proposed framework, simulated results are compared to the measured (where available) or model simulated data (using measurements) for one of the recorded EAF heats. The model used in this paper was validated on approximately 100 heats of measured EAF data. In both cases, equal initial conditions are assumed, including 10 tons of hot heel. Moreover, actuation of the EAF is the same, except for the optimized inputs, i.e., oxygen lancing, carbon injection, and transformer voltage/power. Inputs for slag additives are not optimized as they are controlled properly in the measured data,

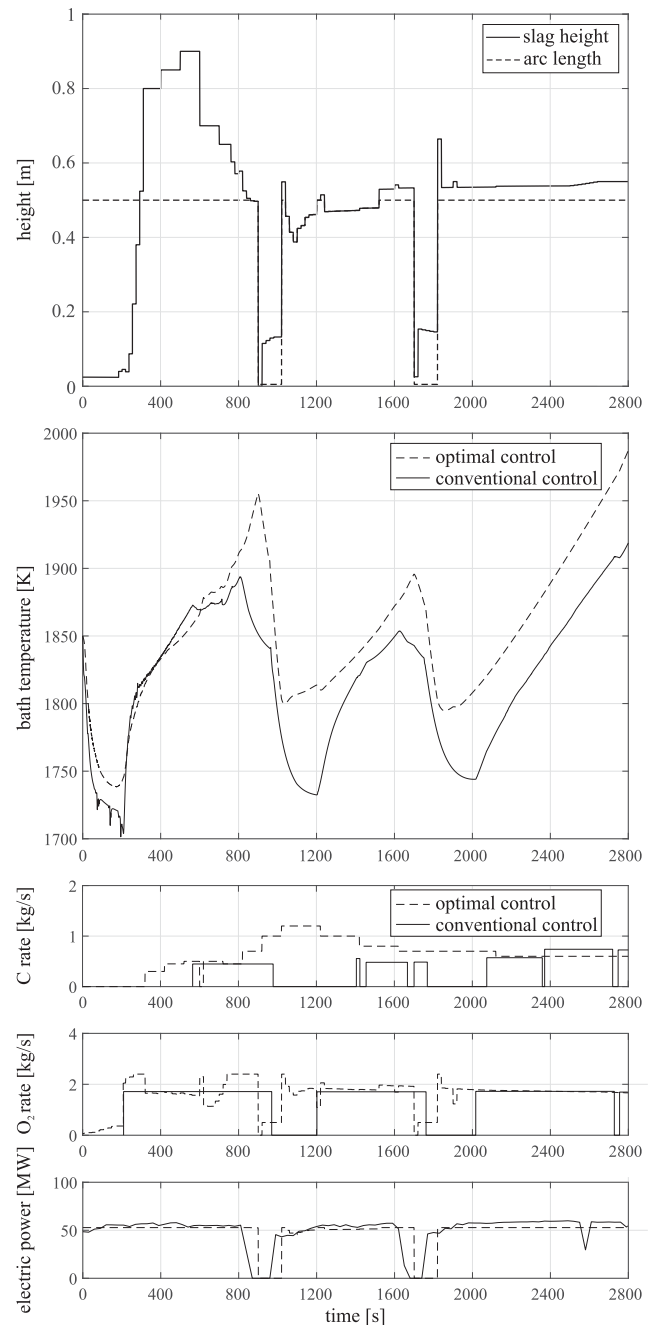


Fig. 3. Simulation of the arc length and slag height (first panel), comparison of the bath temperatures using conventional and optimal EAF control (second panel), and comparison between conventionally and optimally controlled EAF inputs (third to fifth panels).

nor as the inputs for gas burners, as they are not used in real EAF operation. Moreover, optimization of the EAF is carried out using the constraints, assuring that the composition of the steel remains within the desired limits for the refining stage.

As already mentioned, proper slag characteristics need to be assured throughout the melting process in order to achieve its correct height, since it plays a crucial role in the efficiency of the EAF operation. Fig. 3 (first panel) shows the height of the slag and lengths of the arcs when the EAF is actuated according to the proposed optimization algorithm. As can be seen, the

TABLE III
COMPARISON OF THE COSTS BETWEEN CONVENTIONAL AND OPTIMAL CONTROL FOR THE SELECTED HEAT

	at 2800 s		at 38.2 MWh of useful energy	
	con.	opt.	con.	opt.
electrical energy cost [\$]	5867.0	5581.4	5867.0	5097.6
O ₂ cost[\$]	266.6	338.0	266.6	312.0
charged C cost [\$]	195.7	195.7	195.7	195.7
injected C cost [\$]	250.3	486.6	250.3	449.6
slag additives cost [\$]	217	217	217	217
oxidized Fe cost [\$]	294.9	64.4	294.9	48.6
total input costs [\$]	7091.5	6883.1	7091.5	6159.4
useful energy [MWh]	38.2	40.5	38.2	38.2
useful energy cost [\$/kWh]	0.186	0.170	0.186	0.165

lengths of the arcs determined by the optimization procedure are nearly constant. Optimization determines optimal lengths of the arcs in order to achieve the best possible energy transfer to the bath, whilst minimizing the losses.

Furthermore, Fig. 3 (second panel) shows the comparison between liquid steel temperatures when the EAF is actuated using the conventional and the optimized melting profiles. As can be seen, optimized melting profiles lead to higher bath temperature, which is a consequence of increased power intensity to the bath due to the continuously controlled quality of the slag. Finally, Fig. 3 (third to fifth panels) shows the comparison between EAF inputs when the EAF is actuated using the conventional and the optimized melting profiles, which lead to increased EAF efficiency. As shown in third and fourth panels, a very low-rate oxygen flow is engaged soon after the start of the heat; however, a higher rate flow is engaged approximately at the same time as in conventionally actuated heat (measured) in order to prevent furnace wear. Adding too much oxygen too soon can lead to side wall damage; therefore, excessive oxygen rates are limited in the beginning of the heat. Since the furnace operation starts with 10 tons of hot heel, sufficient amount of the initial charge (40 tons) is melted soon after the melting process begins. In this manner, additions of carbon and oxygen can be engaged in order to form foamy slag. Similar conditions appear after charging the second and the third buckets, which are filled less (25 and 20 tons); therefore, the charged scrap is quickly submerged in bath and melted. Also visible, when the second and the third baskets are charged, foamy slag collapses and decreases in height. Since a large amount of the scrap is already in a molten form and due to proper input actuation, the slag quickly foams back to its optimal height. As the fifth panel shows, from the electrical point of view, conventionally and optimally controlled EAF is actuated very similarly, i.e., the differences in electrical power in the beginning of the heat and after each charge are minimal; therefore, the differences in arc lengths and the consequent thermal stress to the EAF vessel are also similar.

Differences between conventional and optimal control of the EAF are also presented in Table III, which shows operational costs at two observations, the first being at 2800 s and the second being at approximately 38 MWh of consumed useful energy, both necessary to achieve the refining stage in a conventional manner.

As shown in Fig. 3 and Table III, differences between both controls of the EAF are clearly visible. The biggest difference between conventional and optimal control is in a much higher rate of carbon (almost 100% more) and a slightly higher rate of oxygen (approximately 25% more) additions, and especially their timely onsets. Observing the conventional control, it can be seen that oxygen is always engaged with the same rate and also with approximately the same delay in relation to charging. Since conventional operation has no information on carbon and oxygen content, ratio between them is most likely inappropriate, leading to a poorer effect on slag foaming.

When observing the costs at 2800 s, it can be seen that optimal control consumes more additives, such as oxygen and carbon; however, less iron is oxidized and less electrical energy is used, which in total leads to lower costs and lower price per kWh of useful energy. It can also be seen that consumed useful energy is approximately 2 MWh higher at the optimally controlled EAF, meaning that the refining stage could be achieved sooner, i.e., at approximately 2500 s, as the bath temperature is sufficient prior to that time (shown in Fig. 3). Therefore, the second observation is made at 38.2 MWh of consumed useful energy, needed to achieve the refining stage. Similarly as before, it is evident that optimal control of the EAF consumes more additives, but less iron is oxidized and less electrical energy is used than in conventional control, which leads to even higher difference in total estimated costs and price per kWh of useful energy. The results, thus, show that the time needed to reach the refining stage and the operational costs of the EAF could be notably shortened. Similar results can also be obtained when using other measured heat data. From the presented results, it can be concluded that the obtained EAF actuation leads to better performance of the EAF while satisfying path and endpoint constraints in terms of the final product as well as the EAF equipment. Furthermore, overall carbon and oxygen consumptions and maximum rates are comparable with other modern EAFs. Finally, actuation of the EAF in terms of transformer powers, oxygen rates, and carbon injections, and their onsets is within the limits of the conventional EAF control, meaning that optimized control of the furnace should not introduce any technology related complications. In order to prove the last statement, a real environment testing needs to be performed. Since more energy is delivered in shorter times, slightly greater temperature derivatives and overall temperatures appear in the furnace, which could lead to higher wear of the furnace; however, extensive real-system testing should prove or negate this assumption. Whether the EAF is not the actual bottleneck in the steel production [25], shorter TTTs and higher energy intensity could be avoided using modifications of the path constraints in the optimization procedure, in order to decrease the waiting time of the EAF and consequential cool-down, leading to unnecessary energy consumption for its reheating.

V. CONCLUSION

This paper presented an EAF optimization framework, designed to increase the efficiency of the EAF through optimized inputs. As shown, proper definition of the optimization

problem can lead to reduced production times and operational costs. Proper control of the selected EAF inputs, i.e., oxygen lancing, carbon injection, and active power, reflected in improved characteristics and proper height of the slag, increased power intensity to the bath and, consequently, higher efficiency of the EAF. Since the results were obtained using a model simulation, savings estimations might be slightly overoptimistic, as the model was always just an approximation of the real system. Even though the model was thoroughly validated, unforeseen conditions can appear, especially when dealing with a system, such as an EAF. Nevertheless, knowing that typical EAF control was performed using a predefined melting profiles and operator's experience, it is clear that such operation of the system is suboptimal; therefore, using a parallel model-based optimization framework can definitely enhance the performance indicators of the EAF.

REFERENCES

- [1] *World Steel in Figures*. Brussels, Belgium: World Steel Assoc., 2017.
- [2] B. Lee and I. Sohn, "Review of innovative energy savings technology for the electric arc furnace," *JOM*, vol. 66, no. 9, p. 1581–1594, 2014.
- [3] H. Ali, K. P. Lynn, and T. M. Aimee, *The State-of-the-Art Clean Technologies (SOACT) for Steelmaking*, 2nd ed. Washington, DC, USA: Amer. Iron Steel Inst., 2010.
- [4] M. Barati, S. Esfahani, and T. A. Utigard, "Energy recovery from high temperature slags," *Energy*, vol. 36, no. 9, pp. 5440–5449, 2011.
- [5] M. Kirschen, V. Risonarta, and H. Pfeifer, "Energy efficiency and the influence of gas burners to the energy related carbon dioxide emissions of electric arc furnaces in steel industry," *Energy*, vol. 34, no. 9, pp. 1065–1072, 2008.
- [6] B. Lee, J. W. Ryu, and I. Sohn, "Effect of hot metal utilization on the steelmaking process parameters in the electric arc furnace," *Steel Res. Int.*, vol. 86, no. 3, pp. 302–309, 2014.
- [7] H. Samet and M. Parniani, "Predictive method for improving SVC speed in electric arc furnace compensation," *IEEE Trans. Power Del.*, vol. 22, no. 1, pp. 732–734, Jan. 2007.
- [8] G. Bisio, G. Rubatto, and R. Martini, "Heat transfer, energy saving and pollution control in UHP electric-arc furnaces," *Energy*, vol. 25, no. 11, pp. 1047–1066, 2000.
- [9] T. Meier *et al.*, "Process modeling and simulation of biochar usage in an electric arc furnace as a substitute for fossil coal," *Steel Res. Int.*, vol. 88, no. 9, 2017, Art. no. 1600458.
- [10] K. Gandt, T. Meier, T. Echterhof, and H. Pfeifer, "Heat recovery from EAF off-gas for steam generation: Analytical exergy study of a sample EAF batch," *Ironmaking Steelmaking*, vol. 43, no. 8, pp. 1–7, 2016.
- [11] J. Cárdenas, A. Conejo, and G. Gnechi, "Metal 2007," in *Proc. 16th Int. Metall. Mater. Conf., Met.*, 2007, pp. 1–7.
- [12] J. Riesbeck, P. Lingebrant, E. Sandberg, and C. Wang, "World renewable energy congress," in *Proc. World Renew. Energy Congr. Conf.*, 2011, pp. 1676–1683.
- [13] J. G. Bekker, I. K. Craig, and P. C. Pistorius, "Model predictive control of an electric arc furnace off-gas process," *Control Eng. Pract.*, vol. 8, no. 4, pp. 445–455, 2000.
- [14] J. G. Bekker, I. K. Craig, and P. C. Pistorius, "Modeling and simulation of an electric arc furnace process," *ISIJ Int.*, vol. 39, no. 1, pp. 23–32, 1999.
- [15] D. J. Oosthuizen, I. K. Craig, and P. C. Pistorius, "Economic evaluation and design of an electric arc furnace controller based on economic objectives," *Control Eng. Pract.*, vol. 12, no. 3, pp. 253–265, 2004.
- [16] D. Wei, I. K. Craig, and M. Bauer, "Multivariate economic performance assessment of an MPC controlled electric arc furnace," *ISA Trans.*, vol. 46, no. 3, pp. 429–436, 2007.
- [17] E.-W. Bai, "Minimizing energy cost in electric arc furnace steel making by optimal control designs," *J. Energy*, vol. 2014, 2014, Art. no. 620695.
- [18] J. J. Snell, *Improved Modeling and Optimal Control of an Electric Arc Furnace*. Iowa, IA, USA: Univ. Iowa, 2010.
- [19] M. Czapla, M. Karbownikczek, and A. Michaliszyn, "The optimisation of electric energy consumption in the electric arc furnace," *Arch. Metall. Mater.*, vol. 53, no. 2, pp. 559–565, 2008.
- [20] R. D. M. MacRosty and C. L. E. Swartz, "Dynamic optimization of electric arc furnace operation," *AIChE J.*, vol. 53, no. 3, pp. 640–653, 2007.
- [21] R. D. M. MacRosty and C. L. E. Swartz, "Dynamic modeling of an industrial electric arc furnace," *Ind. Eng. Chem. Res.*, vol. 44, no. 21, pp. 8067–8083, 2005.
- [22] Y. E. M. Ghobara, *Modeling, Optimization, and Estimation in Electric Arc Furnace (EAF) Operation*. Hamilton, ON, Canada: McMaster Univ., 2013.
- [23] D. Gajić, I. Savić-Gajić, I. Savić, O. Georgieva, and S. Di Gennaro, "Modelling of electrical energy consumption in an electric arc furnace using artificial neural networks," *Energy*, vol. 108, pp. 132–139, 2016.
- [24] A. Fathi, Y. Saboohi, I. Škrjanc, and V. Logar, "Comprehensive electric arc furnace model for simulation purposes and model-based control," *Steel Res. Int.*, vol. 88, no. 3, 2017, Art. no. 1600083.
- [25] D. Gajić, H. Hadera, L. Onofri, I. Harjunkoski, and S. Di Gennaro, "Implementation of an integrated production and electricity optimization system in melt shop," *J. Cleaner Prod.*, vol. 155, no. 1, pp. 39–46, 2017.



Yadollah Saboohi received the B.Sc. degree in engineering from the Queen Mary College, London, U.K., in 1979, the M.Sc. degree in operations research from the London School of Economics, London, U.K., in 1980, and the Ph.D. degree in energy systems engineering from the University of Stuttgart, Stuttgart, Germany, in 1989.

He is currently a Full Professor in energy system engineering with Sharif University of Technology, Tehran, Iran. His main research interests include energy modeling, energy optimization and energy efficiency, energy–environment–water nexus, advanced optimization of energy systems based on exergy analysis, and energy economics.



Amirhossein Fathi received the B.Sc. degree in electrical power engineering from Shiraz University, Shiraz, Iran, in 2008, and the M.Sc. and Ph.D. degrees in energy systems from Sharif University of Technology, Tehran, Iran, in 2010 and 2016, respectively.

In 2014, he was a visiting Ph.D. student at the Laboratory of Modelling, Simulation and Control, Faculty of Electrical Engineering, University of Ljubljana, Ljubljana, Slovenia. His main research interests include modeling, simulation, and advanced control of electric arc furnaces.



Igor Škrjanc received the B.Sc., M.Sc., and Ph.D. degrees in electrical engineering from the Faculty of Electrical and Computer Engineering, University of Ljubljana, Ljubljana, Slovenia, in 1988, 1991, and 1996, respectively.

He is currently a Full Professor with the Faculty of Electrical Engineering and the Head of the Laboratory for Autonomous and Mobile Systems. His main research interests include adaptive, predictive, neuro-fuzzy, and fuzzy adaptive control systems.

Dr. Škrjanc is a Humboldt Research Fellow, a Research Fellow of the Japan Society for the Promotion of Science, and the Chair of Excellence at the University Carlos III of Madrid. He also serves as an Associate Editor for multiple SCIE journals.



Vito Logar received the B.Sc. and Ph.D. degrees in electrical engineering from the Faculty of Electrical Engineering, University of Ljubljana, Ljubljana, Slovenia, in 2004 and 2009, respectively.

He is currently an Assistant Professor with the Faculty of Electrical Engineering. His main research interests include modeling and optimization techniques regarding the electric arc furnace steel recycling processes.

Dr. Logar received the award for outstanding scientific achievements from the Slovenian Research Agency in 2013 and the award for outstanding scientific achievements from the University of Ljubljana in 2014.